Metabolite-sensitive analysis of magnetic resonance spectroscopic signals using the continuous wavelet transform

C Lemke[1], A Schuck Jr.[1,2], J-P Antoine[1] and D M Sima[3]

[1] Institut de recherche en mathématique et physique, Université catholique de Louvain, B-1348 Louvain-la-Neuve, Belgium
[2] Electrical eng. dept. (DELET) at Universidade Federal do Rio Grande do Sul (UFRGS) `http://www.ufrgs.br/delet`, Porto Alegre, RS, Brasil
[3] Electrical Engineering Department, ESAT-SCD/SISTA, Katholieke Universiteit Leuven, B-3001 Leuven, Belgium

E-mail: `jean-pierre.antoine@uclouvain.be`

Abstract. We introduce a new class of wavelets, called metabolite-based autocorrelation wavelets, for the analysis of magnetic resonance spectroscopic MRS) signals by means of the continuous wavelet transform (CWT). Each MRS signal consists of a number of frequency components typical for the active nuclei and the chemical environment around them in a particular voxel. Identifying individual metabolite components is crucial for the evolving field of MRS for clinical applications. In a first step, we develop the theoretical analysis, considering continuous wavelets derived from (Lorentzian lineshape) signal models. With this analytical approach, we can not only tailor individual wavelets but also determine signal parameters such as the damping factor of the Lorentzian lineshape. Then, we design more complex wavelets numerically from discrete metabolite profiles. As the resulting wavelets are discrete, too, they require an extra step of up- and downsampling in order to perform a proper CWT. The outcome is that the present analysis indicates without ambiguity the presence of a given metabolite in a MRS signal.

Keywords: magnetic resonance spectroscopy, metabolites, continuous wavelet transform, metabolite-based autocorrelation wavelets

Submitted to: *Meas. Sci. Technol.*

1. Introduction

In vivo Nuclear Magnetic Resonance Spectroscopy (MRS) is an evolving technique for the non-invasive investigation of metabolites in the human body, especially in the brain. Each MRS signal is a composite of many frequency components typical for the active nuclei and the chemical environment around them in a particular voxel. The number of active nuclei is directly related to the concentration of a certain metabolite in the sample under test [1].

For the clinical use of MRS, it is essential to have a well-working quantitation method. A number of techniques have been proposed, which work either in the time domain or in the frequency domain (see e.g. [2, 3]). Besides, there also exist techniques that analyze a signal in the two domains simultaneously, such as the continuous wavelet transform (CWT) and the Short-Time Fourier transform [4, 5, 6]. A complete survey of wavelet methods in MRS, including the one developed here and references to previous work, may be found in the report [7].

In a series of successive papers from our group [8]-[12], the authors have examined the application of the Morlet CWT to quantitation and compared it to other methods. However, whereas the Morlet wavelet is capable of detecting single peaks in the spectrum of a composite signal and providing parameter estimates to describe these peaks, it cannot separate different metabolite contributions. Now, the Morlet wavelet is standard, but it is not directly related to the analyzed signal. Already in [11], it was pointed out that other wavelets, with more resemblance with the metabolites themselves, should improve the detection. However, instead of choosing known wavelets such as the 'many-humped' ones of Grossmann *et al.* [13], the concept presented here is to *define* wavelet functions directly from the MRS data themselves, by the autocorrelation function of the metabolite profiles, properly averaged to zero. In this way, we obtain wavelets with a spectrum that is very similar to the MRS spectrum and we have a tailor-made tool for signal detection.

Note that band-limited wavelets matching specific signal spectra (not necessarily MRS spectra) have been designed e.g. in [14] and [15], then adapted to the *discrete* wavelet transform (DWT), using an orthonormal multiresolution scheme [16], which is a strong restriction. On the other hand, MRS spectra have been analyzed in [17] with a standard orthonormal DWT. But in both cases, the same difficulties show up. It is true that the DWT is the preferred tool for data compression and signal synthesis, and the most popular in the signal processing community. But the kind of problems treated here can be solved only with the CWT, the DWT is simply not adapted to the analysis process [16, 18, 19]. For instance, both the algorithm for detecting spectral lines [8] and the ridge concept rest upon a stationary phase argument. We recall that a ridge is essentially a line of local maxima in the wavelet transform of a signal. It can be vertical in the case of a singularity, horizontal in the case of a fixed frequency, as here, or neither, in the case of a drifting frequency. The same is true for the determination of the instantaneous frequency [8, 11] and for the subtraction algorithm, that is used for removal of the water (or solvent) peak [4, 5, 6]. All these notions (and other ones) are foreign to the DWT, which is more a signal processing tool. With our approach, on the contrary, we have much more freedom, since we use the CWT. We can choose the best analysing wavelets for the problem at hand and we do not need them to be orthonormal.

On the other hand, it should be noted that autocorrelation wavelets have been considered before, albeit in a totally different context [20, 21, 22]. Namely, these authors evaluate the autocorrelation function of a standard (Daubechies) wavelet, or the corresponding scaling function, and use it for interpolation purposes, all in the framework of a multiresolution analysis based DWT.

As a matter of fact, we have already introduced metabolite-based wavelets in [23] and [24] (see [7] for more details), but they were derived from *simulated* noisefree metabolite profiles, which are constructed from purely Lorentzian shapes. Here, we present new results based on the exploitation of metabolite profiles measured *in vitro*, whose lineshapes also reflect conditions of the particular scanner and measuring

protocol used. We will proceed in two stages. In a first step, we start from a model MRS Free Induction Decay (FID) signal in the time domain, namely, a truncated Lorentzian (i.e., a signal that vanishes for times $t < 0$) and evaluate the performance of the corresponding autocorrelation wavelet. Then, in a second step, we start from real metabolite data. Here, we face the additional problem that data are discrete by the very nature of the acquisition, and thus so is their autocorrelation function. Therefore, an extra step based on interpolation and decimation is needed for using such discrete wavelets for a *continuous* wavelet transform.

As a result, we obtain wavelets that are tailored to the MRS signal to be analyzed. In particular, these wavelets are able to indicate without ambiguity the presence of a given metabolite in a superposition of several metabolites and lipids.

2. Methodology: Metabolite-based autocorrelation wavelets

2.1. Theoretical analysis

Our analysis begins with a model FID signal, we evaluate its autocorrelation function and use the latter as an adapted wavelet after proper normalization.

Given an ergodic process time series $x(\tau)$, its autocorrelation function estimator $R_{xx}(t)$ is defined by

$$R_{xx}(t) = \int_{-\infty}^{\infty} x(\tau)\overline{x(\tau - t)}\,\mathrm{d}\tau\,, \tag{1}$$

where the overbar denotes the complex conjugate [25].

The autocorrelation function in the frequency domain $S_{xx}(\omega)$, i.e., the Fourier transform of $R_{xx}(t)$, is called the autospectrum and can be evaluated by the Wiener-Khintchine relation [25, 26]:

$$S_{xx}(\omega) = \mathcal{F}\left\{R_{xx}(\tau)\right\} = \left|X(\omega)\right|^2. \tag{2}$$

This definition allows us to find the expression of the autocorrelation of a signal, given its spectrum.

To start with, let us take as signal $x(t)$ a one frequency component complex damped exponential function, giving a single Lorentzian spectral line:

$$x(t) = A_1 e^{-D_1 t} e^{i(\omega_1 t + \varphi_1)},\ A_1 > 0,\ D_1 > 0. \tag{3}$$

This signal cannot have an analytical autocorrelation function, since its Fourier transform‡ is a Dirac delta function:

$$X(\omega) = 2\pi A_1 e^{i\varphi_1}\delta(\omega - (\omega_1 + iD_1)). \tag{4}$$

Instead, let us use a slightly changed model $x_1(t)$ (since the phase φ_1 drops out in the autocorrelation function, we omit it):

$$x_1(t) = A_1 e^{-D_1 t} e^{i\omega_1 t}\,\theta(t),\ D > 0, \tag{5}$$

where $\theta(t)$ is the Heaviside step function. We have to consider this type of signals, which vanish for $t < 0$, because this model resembles more a measured FID signal, where there are no available values before the start of the measurement.

Thus, computing the Fourier transform of (5), namely,

$$X_1(\omega) = \frac{A_1}{D_1 + i(\omega - \omega_1)}, \tag{6}$$

‡ We use the asymmetric Fourier transform: $S(\omega) = \int x(t)\, e^{-i\omega t}\ \mathrm{d}t,\ s(t) = \frac{1}{2\pi}\int S(\omega)\, e^{i\omega t}\ \mathrm{d}\omega$.

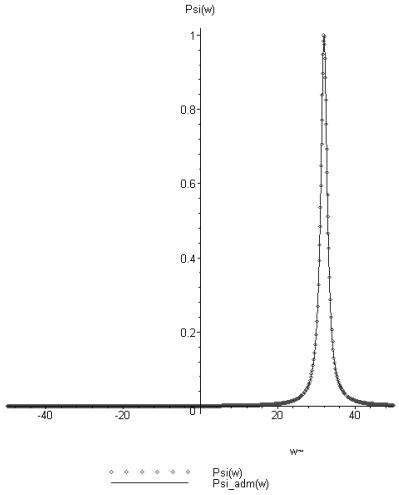


Figure 1: $\Psi_{\rm adm}(\omega) \equiv {\rm Psi}_{\rm adm}({\rm w})$ (solid line) and $\Psi_1(\omega) \equiv {\rm Psi}_1({\rm w})$ (dotted line) for $A_1 = 1$, $D_1 = 1$ and $\omega_1 = 32$ rad/s.

we obtain the autospectrum function of (5) by (2),

$$S_{x_1x_1}(\omega) = \frac{A_1^2}{D_1^2 + (\omega - \omega_1)^2}. \tag{7}$$

Taking the inverse Fourier transform of (7), we obtain the autocorrelation function of (5) given by

$$R_{x_1x_1}(t) = \frac{A_1^2}{2D_1} e^{-D_1|t| + i\omega_1 t},\ -\infty < t < \infty\ . \tag{8}$$

This function is localized and oscillating and can be used as a wavelet function if it is admissible. For all practical purposes, a function ψ is an admissible wavelet only if it has zero mean or, equivalently, its Fourier transform Ψ vanishes at 0, i.e., $\Psi(0) = 0$ [16, 18, 19]. In order to ensure this in our case, it is necessary to introduce an additive correction term, as for the Morlet wavelet. However, the correction term is numerically negligible for realistic values of the parameters, so we will omit it. With this approximation, the wavelet becomes $\psi_1(t) = R_{x_1x_1}(t)$ and, consequently, its Fourier transform is $\Psi_1(\omega) = S_{x_1x_1}(\omega)$. We show in figure 1 the graph of the true wavelet with the correction term, $\Psi_{\rm adm}(\omega)$, and that of $\Psi_1(\omega)$ for $A_1 = 1$, $D_1 = 1$ and $\omega_1 = 32$ rad/s. Indeed there is almost no difference between the two graphs . For arbitrary ω, the value of the correction term is of the order of 10^{-4}. At $\omega = 0$, for instance, the difference between the two functions is 0.0009756, and is thus indeed neglible. It is also interesting to remark that the expressions so obtained are real in the frequency domain and can be easily implemented in numerical softwares.

The CWT of the signal $x(t)$ given in (3) with the wavelet $\psi_1(t)$, evaluated in the frequency domain, is:

$$S_1(b,a) = \frac{1}{2\pi}\sqrt{a}\int_{-\infty}^{\infty} \overline{\Psi_1(a\omega)}\, X(\omega)\, e^{i\omega b}\ {\rm d}\omega \tag{9}$$

$$= \sqrt{a}\ x(b) \frac{A_1^2}{D_1^2 + [\omega_1(a-1) + iaD_1]^2}\ , \tag{10}$$

where $X(\omega)$ denotes the Fourier transform of $x(t)$, and $a > 0$, $b \in \mathbb{R}$ are the dilation and translation variables, respectively.

Clearly this CWT diverges as $a \to 1$ (the match between the wavelet and the signal is too perfect!). By allowing different damping factors for the signal and the wavelet, namely D_{11} and D_1, respectively, we get for $a = 1$:

$$|S_1(b,1)| = e^{-D_{11}b}\,\frac{|A_1^2|}{|D_1^2 - D_{11}^2|}\,. \tag{11}$$

and one can estimate the damping factor of the signal by

$$D_{11} = -\frac{d}{db}\ln|S_1(b,1)|\,. \tag{12}$$

This behavior changes if one has more than one component, i.e., a sum of Lorentzian lineshapes. Take for instance a left truncated signal $x_2(t)$ with two components (we leave out the phases again), such as

$$\begin{aligned} x_2(t) &= \left[A_1 e^{-D_1 t} e^{i\omega_1 t} + A_2 e^{-D_2 t} e^{i\omega_2 t}\right]\theta(t) \\ &\equiv \left[x^{(1)}(t) + x^{(2)}(t)\right]\theta(t), \end{aligned} \tag{13}$$

where $x^{(k)}(t)$, $k = 1, 2$, denotes a single Lorentzian of the form (3), with parameters A_k, D_k, ω_k and $\varphi_k = 0$. The Fourier transform of the signal $x_2(t)$ reads as

$$X_2(\omega) = \frac{A_1}{D_1 + i(\omega - \omega_1)} + \frac{A_2}{D_2 + i(\omega - \omega_2)}\,. \tag{14}$$

The autocorrelation wavelet derived from (14) in the frequency domain is given by

$$\begin{aligned} \Psi_2(\omega) = {} & \frac{A_1^2}{D_1^2 + (\omega - \omega_1)^2} + \frac{A_2^2}{D_2^2 + (\omega - \omega_2)^2} \\ & + \frac{2A_1A_2[D_1D_2 + (\omega - \omega_1)(\omega - \omega_2)]}{[D_1^2 + (\omega - \omega_1)^2][D_2^2 + (\omega - \omega_2)^2]}\,. \end{aligned} \tag{15}$$

If the peaks are sharp enough and far away from each other, the third term in (15) will be numerically negligible and can be ignored. Then, the CWT of the signal $x_2(t)$ using this wavelet becomes

$$\begin{aligned} S_2(b,a) = \sqrt{a}\Bigg\{ & \sum_{k=1}^{2} \frac{A_k^2\, x^{(k)}(b)}{D_k^2 + [a(\omega_k + iD_k) - \omega_k]^2} + \\ & + \frac{A_1^2\, x^{(2)}(b)}{D_1^2 + [a(\omega_2 + iD_2) - \omega_1]^2} \\ & + \frac{A_2^2\, x^{(1)}(b)}{D_2^2 + [a(\omega_1 + iD_1) - \omega_2]^2}\Bigg\}\,. \end{aligned} \tag{16}$$

In real life, however, this assumption might not hold and then other crossing terms could appear in the CWT, making the result somewhat more difficult to interpret. From our experience, two examples of metabolites with such a problem are Myo-inositol (Myo) and Glutamate (Glu).

The first two terms in the sum are similar to (10) and diverge at $a = 1$. Again, choosing different damping factors for the wavelet and signal (namely D_1 and D_2 for the wavelet and D_{11} and D_{22} for the signal), the function will be well-defined for $a = 1$. But in this case, the interaction between two frequencies at this scale generates oscillations in the absolute value of the CWT, so one cannot use it for estimating the damping factors. On the other hand, the last two terms will give local maxima at

scales $a = \omega_j/\omega_k,\ j \neq k$. In this case, assuming again that the peaks are sharp and far enough from each other, and that one has different damping factors for the wavelet and the signal, then the latter can be estimated by

$$D_{11} \approx -\frac{d}{db} \ln |S_2(b, \frac{\omega_2}{\omega_1})| \quad \text{and} \quad D_{22} \approx -\frac{d}{db} \ln |S_2(b, \frac{\omega_1}{\omega_2})|.$$

This method can be further generalized for multipeak signals, but we will refrain from doing it here (see [7] for a detailed analysis). Moreover, the approximations involved in the derivation following (15) may be rather crude in the case of *in vivo* signals, which leads to limited applicability of this theoretical analysis in practice.

Instead, we construct new wavelets for more complex MRS spectra by evaluating realistic metabolite profiles.

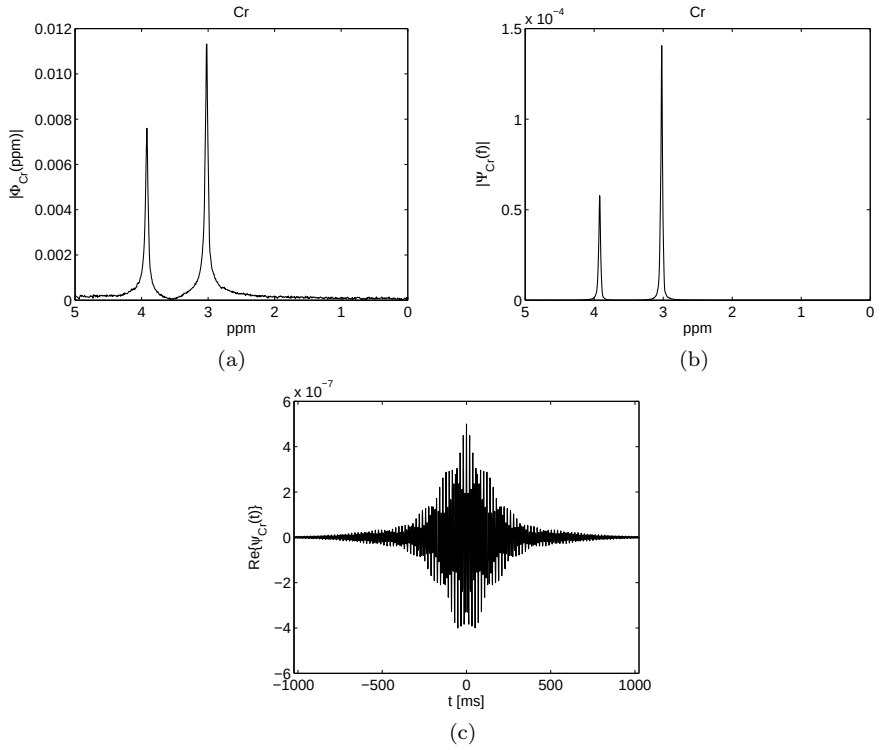


Figure 2: Wavelet constructed from a Creatine (Cr) profile acquired *in vitro*: (a) Modulus of the spectrum of the Cr profile; (b) Modulus of the Cr-based wavelet spectrum; (c) Real part of the Cr-based wavelet in the time domain.

2.2. Data-based signal analysis

Leaving model FID signals behind, we will now exploit the *a priori* information at our disposal and derive our metabolite-based wavelets directly from the available data. These are metabolite profiles that may be acquired by MRS measurements of phantoms filled with single metabolites or by simulation, using tools such as jMRUI [27]. Note that these profiles are, by the very nature of their acquisition, discrete sequences.

We denote the metabolite profiles $\phi_m[n],\ m = 1, \ldots, K$, where K is the number of profiles and the square brackets reflect the discrete indexing of the sequences. Then their autocorrelation function $R_m[n]$ is calculated using the discrete form of $R_{xx}(t)$, namely,

$$R_m[n] = \sum_{k \in \mathbb{Z}} \phi_m[k]\, \overline{\phi_m[k-n]},\ m = 1, \ldots, K, \tag{17}$$

where the overbar denotes the complex conjugate and m indexes the metabolite profiles. They are evaluated as

$$R_m[n] = \mathcal{F}^{-1}\left\{ \left| \mathcal{F}\left\{\phi_m[n]\right\} \right|^2 \right\}; m = 1, \ldots, K, \tag{18}$$

where $\mathcal{F}\{\cdot\}$ denotes the Fourier transform and $\mathcal{F}^{-1}\{\cdot\}$ is the inverse Fourier transform. In practice, they are performed by means of the Fast Fourier Transform (FFT) and its inverse (IFFT). As the metabolite profiles ϕ_m in MRS are a mixture of decaying complex oscillations, their autocorrelation values are complex, too. Since the signals are limited in time, it is enough to remove the mean value of (17) numerically in order to turn these functions into admissible wavelets, namely,

$$\psi_m[n] = R_m[n] - \mathrm{E}\{R_m[n]\},\ \ m = 1, \ldots, K, \tag{19}$$

where m indexes the wavelet function associated to the profile $\phi_m[n]$.

Since these wavelets are designed from a specific metabolite signal, the CWT using one of them is supposed to be more sensitive to the metabolite from which it was derived. In order to show this, we take as an example an *in vitro* Creatine (Cr) profile, that has been acquired on a 1.5 T Philips NT Gyroscan using a PRESS sequence with an echo time of 23 ms and a PRESS box of $2 \times 2 \times 2\,\mathrm{cm}^3$. This profile, originally measured at the University Hospital Leuven, has been provided by ESAT, K.U.Leuven. Figure 2a shows the spectrum of the original Creatine profile, after preprocessing it in order to remove the suppressed water peak and two reference peaks with the method HLSVD-PRO [28], whereas figures 2b and 2c show the spectrum of the derived Cr-based wavelet and its real part in the time domain. Note that both spectra present a pair of very similar characteristic peaks. The wavelet function so obtained is well localized and has zero mean, as required for an admissible wavelet. The same operation is performed for all the metabolites and lipids contained in the database (see Section 3.2 for a detailed analysis example).

The wavelets thus created are numerical and discrete. Using them for performing the CWT involves dilating them, and this requires an extra step based on interpolation and decimation. To that effect, we use an upsampler/downsampler system as proposed in [29]. The rationale is that changing the scale corresponds to choosing another sampling frequency in the discrete case. First, we expand the signal by an integer factor of L by inserting $L-1$ zeros between the original samples and then we calculate these values with a low-pass digital filter with cutoff frequency of π/L rad. We choose a Bartlett window of length $2L-1$ for that. Next, the signal is low-pass filtered again, by a filter with cutoff frequency of π/M rad in order to avoid aliasing effects. For our examples we used a 128 coefficient finite impulse response (FIR) filter in MATLAB®. With this procedure, our possible scales are $a = L/M$. To perform a CWT analysis, the dilated wavelets are created at the desired scales, aligned and their length made equal by zero padding at the endpoints. Then, their spectra are calculated by a FFT. Finally, the CWT is obtained by a discretized version of (9), i.e., by multiplying the spectrum of the signal by the wavelet spectrum and taking the inverse FFT of the result.

3. Analysis results

3.1. Simulated one and two-peak Lorentzian signals

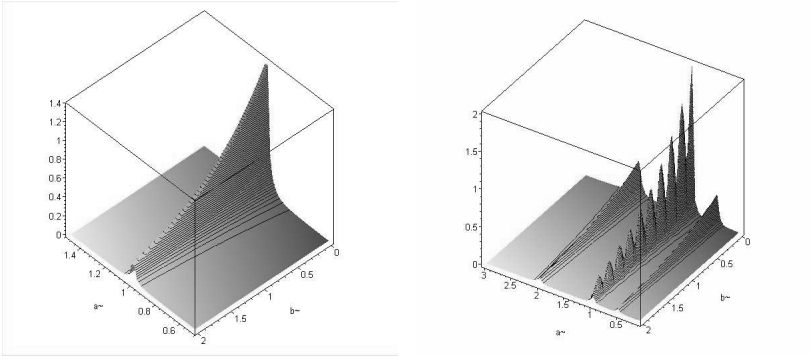
3.1.1. Signals which are not limited in time: Figures 3a and 3b show $|S_L(b,a)|$ for a one peak ($L = 1$) and a two-peak signal ($L = 2$) and wavelets for $A_1 = A_2 = 1$, $D_1 = D_2 = 1$, $\omega_1 = 32$ and $\omega_2 = 64$ rad/s. Notice, in figure 3b, the oscillations resulting from the interference between the two components, as explained at the end of Section 2.1.

3.1.2. Time-limited signals: Now we turn to more realistic signals and apply the method developed above to signals limited in time, that is, vanishing outside some interval $[0, T_0]$, for some finite T_0. First, we analyze numerically a discretized L-component signal $x_L[n]$, defined as

$$x_L[n] = \begin{cases} 0, & 0 \leqslant n \leqslant \frac{N}{4} - 1, \\ \sum_{l=1}^{L} x^{(l)}[n], & \frac{N}{4} \leqslant n \leqslant \frac{3N}{4} - 1, \\ 0, & \frac{3N}{4} \leqslant n \leqslant N - 1, \end{cases} \tag{20}$$

where N is the length of the sampled signal, each $x^{(l)}$ is a single Lorentzian component $x^{(l)}[n] = A_l\, e^{-D_l[n-\frac{N}{4}]t_s}\, e^{i\omega_{sl}[n-\frac{N}{4}]t_s}$, L is the number of components and t_s is the sampling period in seconds. We perform the CWT analysis for the $L = 1$ and the $L = 2$ signal with $N = 4096$ samples using the YAWTB toolbox [31]. The results are shown in figures 4a to 4d.

Both results exhibit strong horizontal ridges (lines of local maxima) for $a = 1$ and this indicates that the component $x^{(1)}$ or $x^{(2)}$ is present in the signal. This feature will be the crucial ingredient for detecting a given signal (pure metabolite) in an unknown superposition. Also, for the two-peak signal and wavelet, one notices the presence of two horizontal ridges at $a = 0.5$ and $a = 2$, which correspond to the ratios between frequencies of the signal and the wavelet.



(a) (b)

Figure 3: $|S_L(b,a)|$ for (a) a one peak signal and wavelet for $A_1 = 1$, $D_1 = 1$, $\omega_1 = 32$ rad/s $b \in [0, 2]$ and $a \in (0, 1.5]$ and, (b) a two-peak signal and wavelet for $A_1 = A_2 = 1$, $D_1 = D_2 = 1$, $\omega_1 = 32$ rad/s and $\omega_2 = 64$ rad/s, $b \in [0, 2]$ and $a \in (0, 3]$.

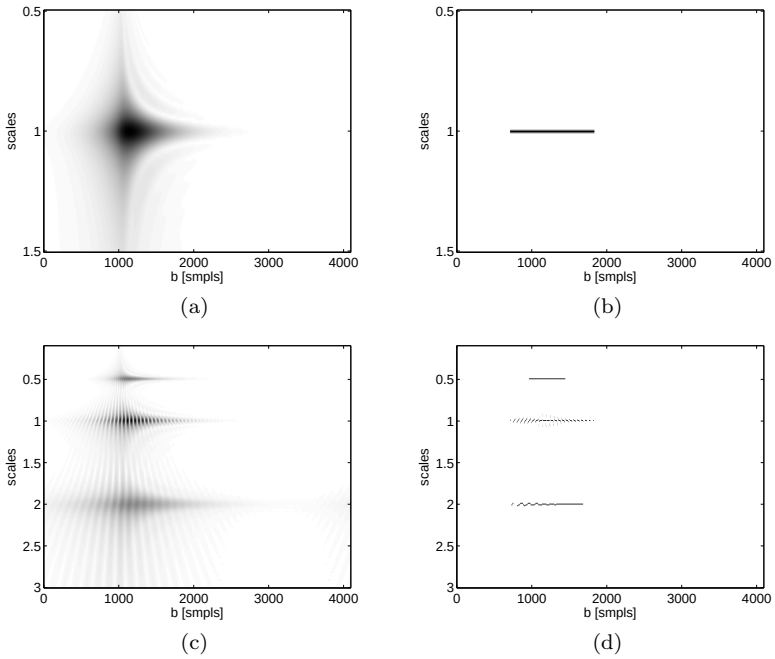


Figure 4: (a) $|CWT\{x_1[n]\}|$ and (b) horizontal ridges of $|CWT\{x_1[n]\}|$; (c) $|CWT\{x_2[n]\}|$ and (d) horizontal ridges of $|CWT\{x_2[n]\}|$for the signal given in (20) with $A_1 = A_2 = 1$, $D_1 = D_2 = 1$, $\omega_1 = 32$ rad/s and $\omega_2 = 64$ rad/s, $t_s = 1/256$ s and $N = 4096$.

3.1.3. Estimation of damping factors: The estimation of damping factors was made for the scales 0.5 and 2 of $|CWT\{x_2[n]\}|$ for $A_1 = A_2 = 1$, $D_{11} = 0.9$ and $D_{22} = 1.1$, $\omega_1 = 32$ rad/s and $\omega_2 = 64$ rad/s, $t_s = 1/256$ s. Here, the signal is zero-padded in order to reduce estimation artifacts before the CWT is performed. The result is shown in figure 5. In the central part of the figure ($5000 \leqslant n \leqslant 6000$), one does obtain the correct values of the damping factors, but for multipeak signals, this estimation proves to be a hard task and more effort should be made on that.

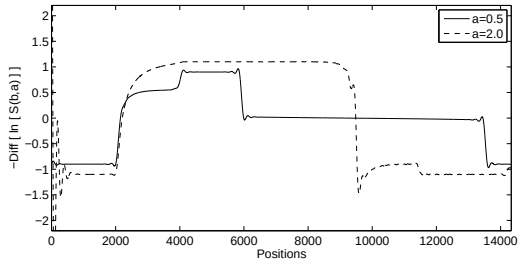


Figure 5: Estimation of damping factors made at the scales $a = 0.5$ (solid line) and $a = 2$ (dashed line) of $|CWT\{x_2[n]\}|$ for $A_1 = A_2 = 1$, $D_{11} = 0.8$ and $D_{22} = 1.2$, $\omega_1 = 32$ rad/s and $\omega_2 = 64$ rad/s, $t_s = 1/256$ s.

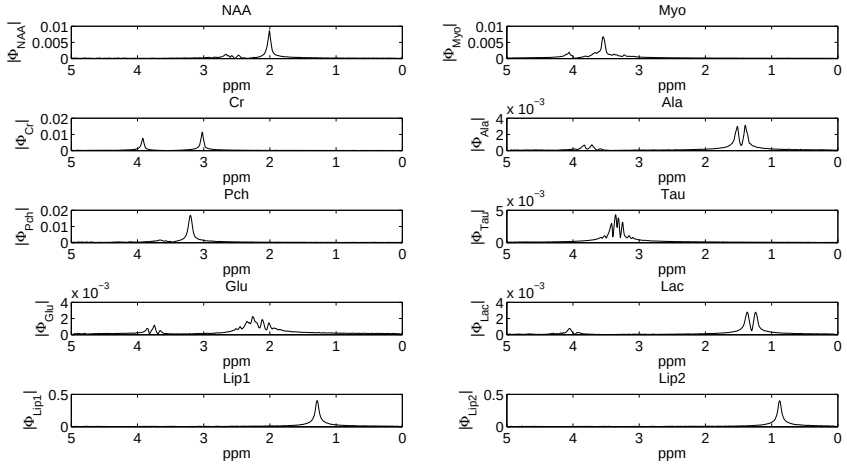


Figure 6: Spectra of eight metabolites measured *in vitro* and two simulated lipids.

3.2. MRS signals acquired in vitro

In the sequel, we explore some examples of analysis exploiting metabolite profiles measured *in vitro*, in the same conditions as the Cr profile described in Section 2.2. The database has been used and described in full detail in [32]. The individual metabolite profiles are shown in figure 6. Note that the two lipids shown are not measured, but derived from a singlet of the Creatine profile. We generate a metabolite-based wavelet for each of the profiles individually. Following [33], we ignore lineshape distortions, baseline and water contributions and describe an MRS signal by

$$s(t) = \sum_{j=1}^{M} s_j(t) + z(t) \equiv \sum_{j=1}^{M} A_j e^{-D_j t}\, e^{i(\omega_j t + \varphi_j)}\, \phi_j(t) + z(t). \qquad (21)$$

The $\phi_j(t)$ are the metabolite profiles measured *in vitro*, M is the number of superposed metabolite signals, D_j is the Lorentzian damping correction, ω_j is the frequency shift, φ_j is the phase shift and A_j is the amplitude factor of the jth modeled metabolite signal. The term $z(t)$ models complex Gaussian white noise. The expression (21) models an *in vivo* signal from the *in vitro* metabolite profiles, provided the parameters chosen for it correspond to the real ones [32].

Using the model (21), we create a signal including all metabolites and lipids from the database, and then three other ones lacking one of the following metabolites: Cr, Lac and NAA, respectively. Table 1 shows the parameters used for this example. The resulting spectra are presented in figure 7. The profile of NAA consists of a single strong peak and a couple of further, but less strong, frequency contributions. Cr has approximately a two peak profile and Lac appears as a doublet with further minor frequency contributions. Note that, in order to show the principle of detecting metabolites in a mixture, we exclude noise from the analysis at this point.

We will now analyze the composite signals with the NAA-, Cr- and Lac-based wavelets. The results are presented in figures 8 to 10. In each figure, the left panels

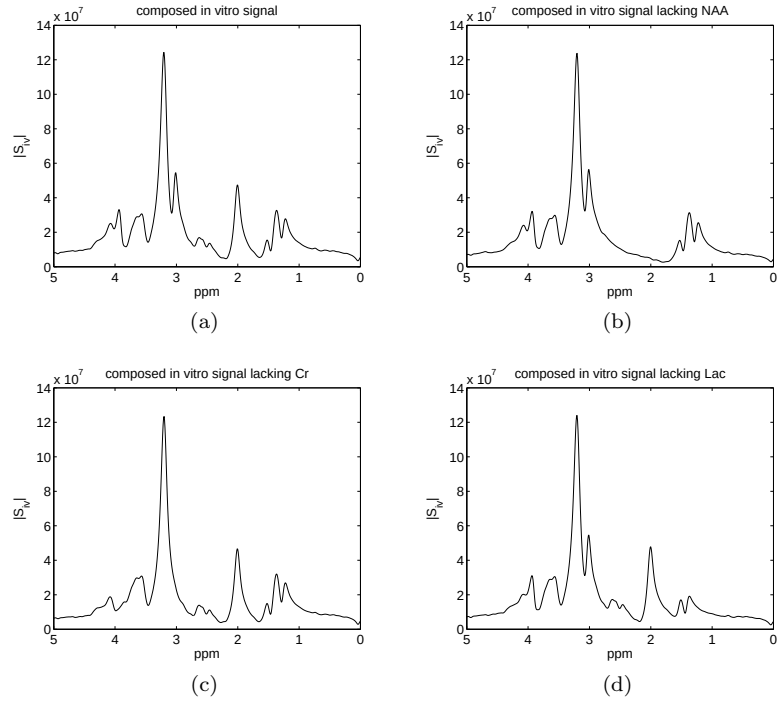


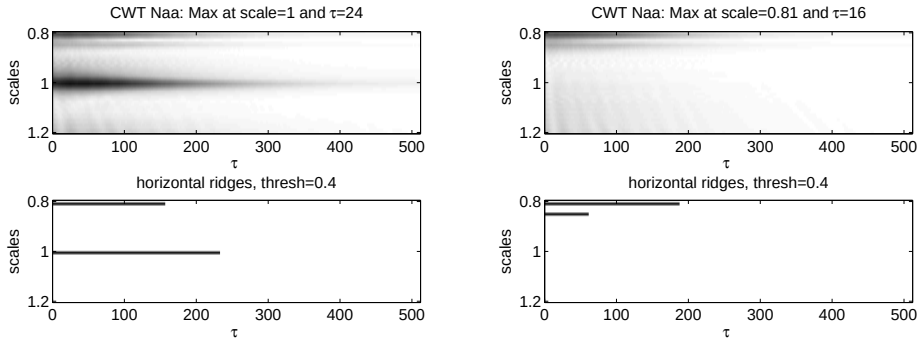
Figure 7: Example of an *in vitro* MRS signal: (a) including all metabolites and lipids from Table 1 and the same signal minus the contribution of (b) NAA, (c) Cr and (d) Lac.

present, on top, the CWT of the composite signal using a metabolite-based wavelet, and, below, the corresponding ridges (lines of maximum modulus). In the same way, the right panels present the CWT and its ridges for the composite signal, but without the metabolite specific to the wavelet used. The grayscale values used are the same for all images.

For NAA, we see a strong ridge at scale $a = 1$ when the metabolite is present (figure 8a). That ridge is no longer present if the NAA contribution is removed from

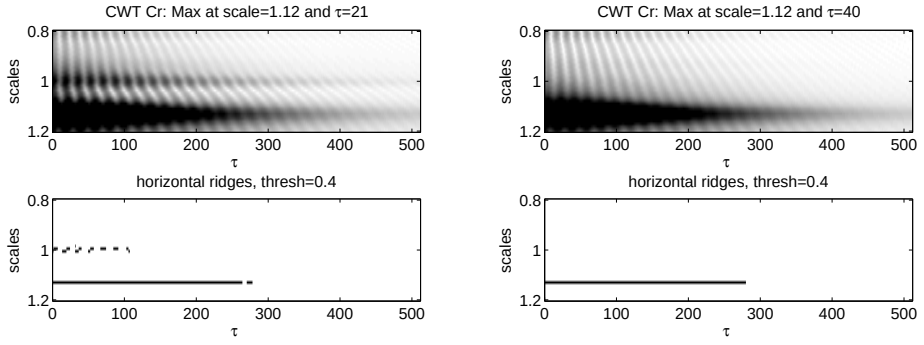
profile	A_j	$D_j[\mathrm{s}^{-1}]$	$\omega_j[\mathrm{rad\,s}^{-1}]$	$\varphi_j[\mathrm{rad}]$
NAA	$1.550 \cdot 10^{10}$	0.012	0	-0.533
Myo	$0.483 \cdot 10^{10}$	0.012	0	-0.533
Cr	$1.121 \cdot 10^{10}$	0.012	0	-0.533
Ala	$1.036 \cdot 10^{10}$	0.012	0	-0.533
Pch	$1.809 \cdot 10^{10}$	0.012	0	-0.533
Tau	$0.004 \cdot 10^{9}$	0.012	0	-0.533
Glu	$0.085 \cdot 10^{9}$	0.012	0	-0.533
Lac	$1.568 \cdot 10^{10}$	0.012	0	-0.533
Lip1	$0.239 \cdot 10^{6}$	0.012	0	-0.533
Lip2	$0.123 \cdot 10^{4}$	0.012	0	-0.533

Table 1: Parameter values used in (21) for the simulation of the example *in vitro* MRS signal.



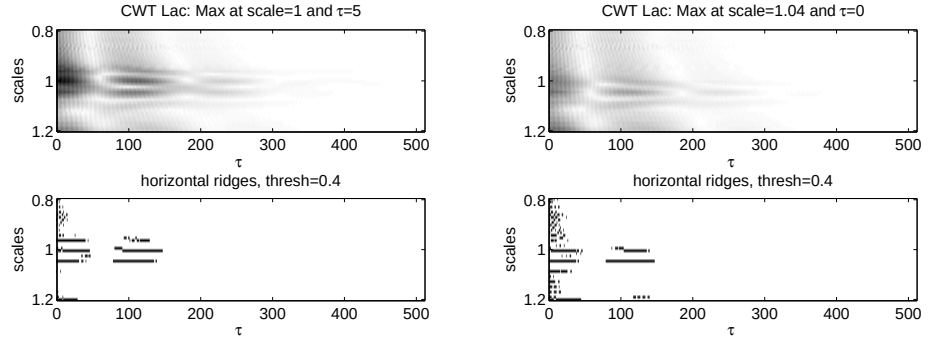
(a) (b)

Figure 8: CWT using the *in vitro* NAA-wavelet on (a) the composite signal from figure 7a and (b) the composite signal lacking the NAA contribution.



(a) (b)

Figure 9: CWT using the *in vitro* Cr-wavelet on (a) the composite signal from figure 7a and (b) the composite signal lacking the Cr contribution.



(a) (b)

Figure 10: CWT using the *in vitro* Lac-wavelet on (a) on the composite signal from Figure 7a and (b) on the composite signal lacking the Lac contribution.

the signal (figure 8b). The results for Cr in figure 9 are similar. If Cr is contained in the composite signal, we see a strong contribution at scale $a = 1$, which disappears if Cr is removed. In the case of Lac (figure 10), the results are similar to those of Cr, but not as clear. Local maxima appear at scale $a = 1.04$, they are weak but unquestionably present. They do indicate the contribution of Alanine, whose spectrum is very similar to the Lactate profile (see figure 6). Consequently, it is difficult to distinguish between the two metabolite profiles in practice.

Depending on how strongly a metabolite signal contributes to the mixture, the detection of the metabolite will be working down to a certain Signal-to-Noise Ratio (SNR). Considering complex Gaussian white noise, we are able to repeat the Cr-example with similar good results down to a SNR of 0 dB. For the detection of Lac in our example, on the other hand, the SNR should be higher than 6 dB.

The results presented here for the metabolite-based wavelets were obtained using wavelets based on metabolite profiles measured *in vitro*. They display the same characteristics as the analysis with completely simulated metabolite profiles and MRS signals, as we have already demonstrated in [23] and [24] and thus confirm our previous findings.

4. Conclusion

In this paper, we have presented a new class of wavelets, which we call metabolite-based autocorrelation wavelets, and which allow one to tailor the analysis of MRS signals for specific metabolites. Deriving wavelets from Lorentzian models provides the theoretical and analytical basis for wavelets designed to analyze complex signals.

The simplest starting point is a single peak spectrum, namely a damped, truncated Lorentzian function, from which we obtain a wavelet which is similar to the standard Morlet wavelet. However, we are able to extend the analysis to much more complicated signals. We can derive a wavelet from a multi-peak Lorentzian model and thus adapt the wavelet to the metabolite spectrum we are interested in. In this way, we overcome the inherent limitation of the standard Morlet wavelet, which analyzes each frequency component of data separately. Using wavelets derived from the autocorrelation of the Lorentzian model, we can estimate signal parameters like the damping factor, because the solution is analytical. The estimation is comparable to exploiting the Morlet wavelet as in [12].

Unfortunately, the analytical determination of signal parameters is practically lost when we derive wavelets numerically from true metabolite profiles. In principle, it is possible to estimate the amplitude from (21), thus measure the contribution of the given metabolite and then evaluate it by means of a Monte-Carlo simulation, as described in [7]. Given that the CWT of the pure metabolite signal is known, one can obtain the amplitude from the ratio of the CWT of the MRS signal to the pure CWT analysis. However, this approach is both very rough and limited at the moment to a small number of metabolites and it would need further extension to become a reliable estimation method.

Anyway, a metabolite-based autocorrelation wavelet matches extremely well a specific metabolite spectrum. So it is good at detecting the presence of a specific metabolite in an MRS signal by comparing the response at the scale $a = 1$ with other scales, because it exploits *a priori* knowledge optimally. However, the prerequisite for the method to be efficient is that the profiles differ significantly enough, as we have shown by referring to Lac, NAA and Cr. Differentiating between Lac and Alanine

(Ala), for instance, is difficult, since the spectra are too similar. Future work might combine Lac- and Ala-based wavelet analysis results for an enhanced disentangling of the two metabolites.

In conclusion, our approach provides us with a tool for a metabolite specific analysis of a MRS signal. Open issues are a fully automated detection algorithm and a robust parameter estimation for the wavelets based on metabolite profiles. Then, the information gained from our metabolite specific analysis should be combined with existing quantitation methods and the potential improvement in quantifying metabolite contributions should be investigated.

Acknowledgments

This work is part of the Advanced Signal Processing for Ultra-fast Magnetic Resonance (FAST) project funded by the Marie-Curie Research Network (MRTN-CT-2006-035801) http://fast-mrs.eu. C Lemke was until January, 2010, an ER Marie-Curie Fellow. A Schuck Jr. thanks the Conselho Nacional de Pesquisa e Desenvolvimento - CNPq, Brazil, for its financial support. D M Sima acknowledges a postdoctoral fellowship from the Fund for Scientific Research Flanders. The authors would also like to express their gratitude to Professor S van Huffel, and M I Osorio Garcia (K.U. Leuven), and Professor D van Ormondt (TU Delft) for fruitful discussions and their invaluable advice. They also thank the anonymous referees for their constructive criticisms that have substantially clarified several points of the paper.

References

[1] Hornak J-P 1997 *The Basics of NMR*. Department of Chemistry, Rochester Institute of Technology, Rochester, NY. `http://www.cis.rit.edu/htbooks/nmr/`

[2] Poullet J-B, Sima, D M and Van Huffel, S 2008 MRS signal quantitation: A review of time- and frequency-domain methods, *J. Magn. Reson. A*, **195** 134–44

[3] Mierisová S and Ala-Korpela M 2001 MR spectroscopy quantitation: a review of frequency domain methods *NMR Biomed.* **14** 247–59

[4] Barache D, Antoine J-P and Dereppe J-M 1997 The continuous wavelet transform, an analysis tool for NMR spectroscopy *J. Magn. Reson. A* **128** 1–11

[5] Antoine J-P, Coron A, and Chauvin C 2001 Wavelets and related time-frequency techniques in magnetic resonance spectroscopy *NMR Biomed.* **14** 265–270

[6] Antoine J-P and Coron A 2001 Time-frequency and time-scale approach to magnetic resonance spectroscopy *J. Comput. Methods in Science & Engineering (JCMSE)* **1** 327–52

[7] Suvichakorn A, Lemke C, Schuck Jr A and Antoine J-P 2010 The continuous wavelet transform in MRS, Tutorial text, *Marie Curie Research Training Network FAST*. `http://www.fast-mariecurie-rtn-project.eu/#Wavelet`

[8] Suvichakorn A and Antoine J-P 2008 Analyzing NMR Spectra with the Morlet wavelet *Proc. EUSIPCO 2008, Lausanne, Switzerland*, paper # 1569102372

[9] Suvichakorn A, Ratiney H, Bucur A, Cavassila S and Antoine J-P 2008 quantitation method using the Morlet wavelet for magnetic resonance spectroscopic signals with macromolecular contamination *Proc. IEEE EMBC 08 (Vancouver, BC, Canada)* pp. 2681-4

[10] Suvichakorn A, Ratiney H, Bucur A, Cavassila S and Antoine J-P 2008 Morlet wavelet analysis of magnetic resonance spectroscopic signals with macromolecular contamination *Proc. IEEE IST 2008 (Chania, Greece)*, pp. 321–5

[11] Suvichakorn A, Ratiney H, Bucur A, Cavassila S and Antoine J-P 2009 Toward a quantitative analysis of *in vivo* proton magnetic resonance spectroscopic signals using the continuous Morlet wavelet transform *Meas. Sci. Technol.* **20** paper #104029

[12] Suvichakorn A, Ratiney H, Cavassila S and Antoine J-P 2010 Wavelet-based techniques in MRS Chapter 9 in *Signal Processing*, pp. 167–196 ; S. Miron (ed.), IN-TECH, Vienna, Austria, and Rijeka, Croatia

[13] Grossmann A, Kronland-Martinet R, and Morlet J 1990 Reading and understanding continuous wavelet transforms, in Combes J-M, Grossmann A and Tchamitchian P, editors *Wavelets, Time-Frequency Methods and Phase Space (Proc. Marseille 1987), 2d ed.*, 2–20) (Springer-Verlag, Berlin)
[14] Chapa J O and Rao R M 2000 Algorithms for designing wavelets to match a specified signal *IEEE Trans. Signal Process.*, **48** 3395-406
[15] Bahrampour A R, Izadnia S and Vahedi M 2008 A variational method for designing wavelets to match a specified signal *Signal Process.*, **88** 2417–24
[16] Daubechies I 1992 *Ten Lectures on Wavelets*, (Philadelphia, PA: SIAM)
[17] Neue G 1996 Simplification of dynamical NMR spectroscopy by wavelet transform *Solid State Nucl. Magn. Reson.* **5** 305–14
[18] Torrésani B 1995 *Analyse continue par ondelettes* (Paris: InterEditions & CNRS Editions)
[19] Antoine J-P, Murenzi R, Vandergheynst P and Ali S T 2004 *Two-Dimensional Wavelets and their Relatives* (Cambridge, UK: Cambridge University Press)
[20] Shensa M J 1992 The discrete wavelet transform: Wedding the à trous and the Mallat algorithms *IEEE Trans. Signal Process.* **40** 2464–82
[21] Saito N and Beylkin G 1993 Multiresolution representations using the auto-correlation functions of compactly supported wavelets *IEEE Trans. Signal Process.* **41** 3584-90
[22] Beylkin G and Torrésani B 1996 Implementation of operators via filter banks — Hardy wavelets and autocorrelation shell, *Applied Comput. Harmon. Anal.* **3** 164–85
[23] Lemke C, Schuck A, Antoine J-P, Sima D M and Osorio Garcia M I 2010 Metabolite-based wavelets for analyzing magnetic resonance spectroscopic signals *Proc. IEEE IST 2010 (Thessaloniki, Greece)* pp. 357-60
[24] Schuck A, Lemke C, Suvichakorn A and Antoine J-P 2010 Analysis of magnetic resonance spectroscopic signals with data-based autocorrelation wavelets *Proc. IEEE EMBC 2010 (Buenos Aires, Argentina)*, pp.855-8
[25] Papoulis A and Pillai SU 2002 *Probability, Random Variables and Stochastic Processes* (New York: McGraw-Hill, 4th edition)
[26] Bendat J S and Piersol A G 2000 *Random Data: Analysis and Measurement Procedures* (New York: J.Wiley, 3rd edition)
[27] For jMRUI, see `http://sermn02.uab.cat/mrui/mruiOverview.shtml`
[28] Laudadio T, Mastronardi N, Vanhamme L, Van Hecke P, and Van Huffel S 2002 Improved Lanczos algorithms for blackbox MRS data quantitation *J. Magn. Reson.* **157** 292–7
[29] Oppenheim A, Schaffer R W and Buck J R 1999 *Discrete-Time Signal Processing* (Englewood Cliffs, NJ: Prentice-Hall, 2nd edition)
[30] Graveron-Demilly D, Diop A, Briguet A and Fenet B 1993 Product-operator algebra for strongly coupled spin systems *J. Magn. Reson. A* **101** 233–9
[31] Jacques L, Coron A, Vandergheynst P and Rivoldini A 2007 The YAWTb toolbox : Yet Another Wavelet Toolbox. `http://rhea.tele.ucl.ac.be/yawtb`
[32] Poullet J-B, Sima D M, Simonetti A W, De Neuter B, Vanhamme L, Lemmerling P and Van Huffel S 2007 An automated quantitation of short echo time MRS spectra in an open source software environment: AQSES *NMR Biomed.* **20** 493–504
[33] Sima D M, Osorio Garcia M I, Poullet J-B, Suvichakorn A, Antoine J-P, Van Huffel S and van Ormondt D 2009 Lineshape estimation for magnetic resonance spectroscopy (MRS) signals: self-deconvolution revisited *Meas. Sci. Technol.* **20** paper #104031